Yield Strength Ratio and Liquefaction Analysis of Slopes and Embankments

Scott M. Olson, A.M.ASCE,[1] and Timothy D. Stark, M.ASCE[2]

Abstract: A procedure is proposed to evaluate the triggering of liquefaction in ground subjected to a static shear stress, i.e., sloping ground, using the yield strength ratio, $s_u(\text{yield})/\sigma'_{v0}$. Thirty liquefaction flow failures were back analyzed to evaluate shear strengths and strength ratios mobilized at the triggering of liquefaction. Strength ratios mobilized during the static liquefaction flow failures ranged from approximately 0.24 to 0.30 and are correlated to corrected cone and standard penetration resistances. These yield strength ratios and previously published liquefied strength ratios are used to develop a comprehensive liquefaction analysis for ground subjected to a static shear stress. This analysis addresses: (1) liquefaction susceptibility; (2) liquefaction triggering; and (3) post-triggering/flow failure stability. In particular, step (2) uses the yield strength ratio back-calculated from flow failure case histories and the cyclic stress method to incorporate seismic loading.

DOI: 10.1061/(ASCE)1090-0241(2003)129:8(727)

CE Database subject headings: Liquefaction; Slopes; Embankments; Shear strength.

Introduction

A liquefaction analysis for ground subjected to a static shear stress, i.e., slopes, embankments, or foundations of structures, typically consists of three primary tasks: (1) a susceptibility analysis; (2) a triggering analysis; and (3) a post-triggering/flow failure stability analysis. A liquefaction susceptibility analysis determines whether a given soil deposit is in a contractive state, i.e., susceptible to undrained strain-softening behavior and flow failure. Numerous investigators (e.g., Sladen and Hewitt 1989; Ishihara 1993; Fear and Robertson 1995; Baziar and Dobry 1995) have proposed susceptibility boundary lines between penetration resistance (a measure of soil density) and effective confining stress to separate contractive from dilative soil states. Similarly, procedures are available to evaluate the liquefied shear strength for use in a post-triggering/flow failure stability analysis. Olson and Stark (2002) proposed a procedure to estimate the liquefied strength ratio, $s_u(\text{LIQ})/\sigma'_{v0}$, using the corrected cone penetration test (CPT) or the standard penetration test (SPT) resistance. The liquefied strength ratio can be used in a post-triggering stability analysis.

In contrast, few procedures are available to evaluate the triggering of liquefaction in ground subjected to a static shear stress. The two most widely known procedures are those of Poulos et al. (1985a) and Seed and Harder (1990). The Poulos et al. (1985a) procedure compares the shear strain induced by loading (static or seismic) to the shear strain required to trigger undrained strain-softening response. Poulos et al. (1985b) and Poulos (1988) concluded that practically any induced shear strain will be sufficient to trigger liquefaction in nonplastic soils, while soils with some plasticity can accommodate a finite shear strain prior to reaching their yield (or peak) shear strength. However, a suite of laboratory tests are necessary to estimate the induced shear strains for a given loading, and Poulos et al. (1985b) and Poulos (1988) indicated that laboratory measured shear strains may not resemble shear strains induced in situ, particularly for nonplastic soils. For these reasons, this procedure is difficult to apply in many practical situations.

Seed and Harder (1990) presented an extension to the SPT based level ground liquefaction analysis procedure (Seed et al. 1985) to evaluate triggering of liquefaction in ground subjected to a static shear stress. Seed and Harder (1990) proposed correction factors, K_α and K_σ, to modify the level ground cyclic resistance ratio to account for a static shear stress and an overburden stress greater than 100 kPa, respectively. Despite Harder and Boulanger's (1997) update, the correction factors exhibit large scatter resulting in uncertainty in their application. Consequently, the corrections are sometimes omitted on small and moderately sized projects, or expensive site-specific corrections are developed for large projects (e.g., Pillai and Stewart 1994; Hedien et al. 1998).

This paper presents a procedure to evaluate the triggering of liquefaction in ground subjected to a static shear stress using the yield (or peak) strength ratio back-calculated from available static loading- and deformation-induced liquefaction flow failures. The procedure is illustrated using available seismically induced flow failures. The proposed triggering analysis does not require a suite of laboratory tests or correction factors (K_α and K_σ), and is incorporated into a comprehensive procedure to evaluate: (1) liquefaction susceptibility; (2) liquefaction triggering; and (3) post-triggering/flow failure stability.

[1]Project Manager, URS Corporation, 1001 Highlands Plaza Dr. West, Suite 300, St. Louis, MO 63110. E-mail: scott_olson@urscorp.com

[2]Professor of Civil and Environmental Engineering, Univ. of Illinois-Urbana-Champaign, Dept. of Civil and Environmental Engineering, Urbana, IL 61801.

Note. Discussion open until January 1, 2004. Separate discussions must be submitted for individual papers. To extend the closing date by one month, a written request must be filed with the ASCE Managing Editor. The manuscript for this paper was submitted for review and possible publication on August 18, 2000; approved on October 20, 2002. This paper is part of the ***Journal of Geotechnical and Geoenvironmental Engineering***, Vol. 129, No. 8, August 1, 2003. ©ASCE, ISSN 1090-0241/2003/8-727–737/$18.00.

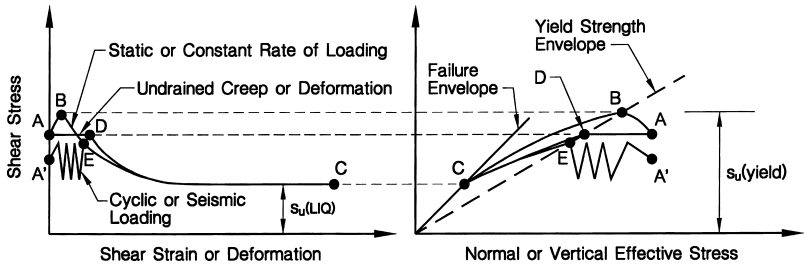

Fig. 1. Schematic undrained response of saturated, contractive sandy soil

Yield Shear Strength and Yield Strength Ratio

Fig. 1 schematically presents the behavior of saturated, contractive, sandy soil during undrained loading. The yield shear strength [s_u(yield)] is defined as the peak shear strength available during undrained loading (Terzaghi et al. 1996). Undrained strain softening can be triggered by either static or dynamic loads, or by deformation under a static shear stress that is larger than the liquefied shear strength. As demonstrated by Eckersley (1990) and Sasitharan et al. (1993), loading can be completely drained prior to the triggering of undrained strain softening response.

Hanzawa et al. (1979) measured peak shear strengths from consolidated-undrained triaxial compression tests on saturated, contractive sand specimens tested at the same void ratio but various effective confining pressures. These peak shear strengths produced an approximately linear peak shear strength envelope in stress path space. Hanzawa (1980) then used this peak strength envelope to evaluate liquefaction triggering in a loose, sandy soil underlying an embankment.

Since 1980, numerous investigators have presented similar results and proposed various names for the envelope of peak shear strengths and the surface that defines the stress path followed during undrained strain softening (e.g., Vaid and Chern 1985; Sladen et al. 1985; Sasitharan et al. 1993; among others). Herein, this line of yield (or peak) shear strengths is denoted the ''yield strength envelope'' because it defines the stress conditions at which the yield shear strength is mobilized.

The yield strength ratio is defined as the yield shear strength normalized by the prefailure vertical effective stress, $s_u(\text{yield})/\sigma'_{v0}$. The yield strength ratio is nearly equivalent to the inclination of the yield strength envelope, expressed as

$$\frac{s_u(\text{yield})}{\sigma'_{v0}} \approx \tan \phi_y \tag{1}$$

where ϕ_y=mobilized yield friction angle (in a Mohr–Coulomb diagram). The difference in these parameters is that the yield strength envelope uses the normal effective stress while the yield strength ratio uses the vertical effective stress. However, for the large majority of the flow failures studied herein, the portion of the initial (yield) failure surface within the zone of liquefaction approximates direct simple shear conditions. Thus for most flow failure, the difference between vertical effective stress and normal effective stress may be minimal.

Back Analysis of Flow Failure Case Histories

Olson (2001) examined 33 liquefaction flow failure case histories available in the literature. Olson (2001) divided the flow failures into three categories: (1) static loading-induced failures; (2) deformation-induced failures; and (3) seismically induced failures. Only static loading-induced failures can be used confidently to assess the yield shear strength and strength ratio because the shear strength back-calculated from the prefailure geometry corresponds directly to the yield strength envelope.

To illustrate this concept, consider an element within a saturated, loose sandy deposit either within or underlying an embankment during construction. Point A in Fig. 1 represents the prevailing stress and strain conditions in the element. Point A could have been reached by drained, partially drained, or completely undrained loading during embankment construction. During placement of the next fill lift, the element moves from Point A to Point B, which is located on the yield strength envelope. This step assumes that the drainage boundaries and permeability of the element result in the fill lift causing a temporary undrained condition in the element. Point B represents the maximum shear resistance that the soil element can mobilize under undrained conditions. When the shear stress in this element induced by the embankment attempts to exceed Point B (the yield shear strength), the loose soil structure yields and collapses, and liquefaction is triggered. The element then moves from Point B to Point C, the liquefied shear strength. Therefore, for cases of static loading-induced flow failure, the shear stress mobilized in the zone of contractive soil immediately prior to failure is approximately equal to the yield shear strength. A limit-equilibrium stability analysis of the prefailure geometry provides a reasonable estimate of the yield shear strength and strength ratio mobilized within the zone of liquefaction.

To illustrate conditions leading to deformation-induced failure, again consider a soil element with stress and strain conditions represented by Point A in Fig. 1. Point A could have been reached by drained or undrained loading, and the static shear stress carried by the element (Point A) is greater than its liquefied shear strength (Point C). In this case, the static shear stress resulting from the embankment is large enough to initiate shear strain, creep, or another deformation mechanism within the embankment and/or foundation. If the shear deformation is large enough and element A is undrained, the element moves horizontally from Point A to Point D, which is located on the yield strength envelope. At Point D, liquefaction is triggered, and the element moves from Point D to Point C, the liquefied shear strength. As shown in Fig. 1, the shear stress and stress ratio represented by Point A are less than the yield shear strength and strength ratio at the prefailure effective stress, respectively. Therefore, the shear stress and stress ratio obtained from a limit-equilibrium analysis of the prefailure geometry in a deformation-induced failure may be less than the yield shear strength and strength ratio, respectively. However, as indicated subsequently, several deformation-induced flow failures exhibit prefailure shear stress and stress ratio conditions that correspond closely to the yield shear strength and strength ratio. This

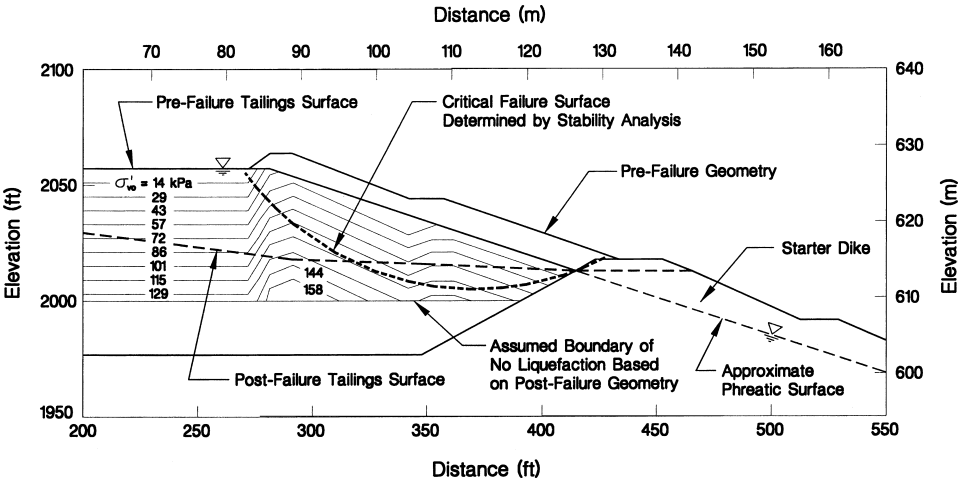

Fig. 2. Prefailure vertical effective stress contours and critical failure surface used for yield strength analysis of Mochi-Koshi Tailings Dam No. 1

occurs in cases where the deformation that triggered liquefaction occurred simultaneously with fill placement during construction.

Seismically induced flow failures also generally do not represent stress conditions that correspond to the yield shear strength and strength ratio. To illustrate this, consider a soil element with stress and strain conditions represented by Point A′ in Fig. 1. Point A′ could have been reached by drained or undrained loading, and the static shear stress carried by the element is greater than its liquefied shear strength. The element is then subjected to a seismic or dynamic load. If the duration and intensity of the seismic/dynamic load is sufficient to cause porewater pressure buildup that moves the element from Point A′ to Point E, liquefaction is triggered, and the element moves from Point E to Point C. The shear stress and stress ratio represented by Point A′ are less than the yield shear strength and strength ratio at the prefailure effective stress, respectively. Therefore, the shear stress and stress ratio obtained from a limit-equilibrium analysis of the prefailure geometry may be less than the yield shear strength and strength ratio.

Procedure to Back Calculate Prefailure Strength Ratio

Olson (2001) presents a procedure to back-calculate the prefailure strength ratio of slopes and embankments. As indicated above, the prefailure strength ratios obtained from static loading- and several deformation-induced flow failure case histories correspond to the yield strength ratio. In contrast, the prefailure strength ratio back-calculated from seismically induced failures generally is smaller than the yield strength ratio.

In this procedure, the approximate zone of contractive, liquefiable soil must be known or estimated. Contours of equal prefailure vertical effective stress were determined within the zone of liquefaction, as illustrated in Fig. 2 for Mochi Koshi Tailings Dam 1 (Ishihara 1984). Using a trial value of strength ratio, different values of shear strength were assigned to each vertical effective stress contour in the zone of liquefaction. Using the failure surface search option of *UTEXAS3* (Wright 1992) and Spencer's (1967) stability method, the critical initial circular or noncircular failure surface was identified. The strength ratio was then varied (which in turn varies the shear strength mobilized below each σ'_{v0} contour within the zone of liquefaction) until a factor of safety of unity was achieved. Assumptions regarding the shear strengths of nonliquefied soils and the dimensions of the zone of liquefaction resulted in a range of strength ratios for each case. The drained or undrained shear strengths of all of the soils were assumed to be fully mobilized, i.e., progressive failure was not considered. Olson (2001) details the shear strengths of the nonliquefied soils and the dimensions of the liquefied zones for each case history.

This analysis considers the entire range of prefailure vertical effective stress controlling the shear strength mobilized at the triggering of liquefaction. For subsequent interpretations, it was useful to determine a weighted average prefailure vertical effective stress along the critical failure surface. The critical failure surface was divided into a number of segments, and the weighted average vertical effective stress within the zone of liquefaction was determined as

$$\sigma'_{v0}(\text{ave}) = \frac{\Sigma_{i=1}^{n} \sigma'_{v,i} \cdot L_i}{\Sigma_{i=1}^{n} L_i} \tag{2}$$

where $\sigma'_{v,i}$=vertical effective stress; and L_i=length of segment i of the critical failure surface. Eq. (2) also was used to calculate a weighted average vertical total stress $[\sigma_{v0}(\text{ave})]$ for the seismically induced failures by substituting the vertical total stress of segment i, $\sigma_{v,i}$, for $\sigma'_{v,i}$ in Eq. (2).

For nearly all of the cases studied, Olson (2001) also evaluated trial failure surfaces based on descriptions of the failure, eyewitness accounts, and postfailure morphology (i.e., locations of broken pavement, intact portions of embankments, etc.). In most cases, these trial failure surfaces closely resembled the critical failure surface calculated using *UTEXAS3*. In cases where the trial and critical failure surfaces differed considerably, we incorporated results from both failure surfaces into the reported range of strength ratios and shear strengths. Olson (2001) presents the details of the analyses and assumptions for each case history.

Procedure to Back Calculate Prefailure Shear Strength

This study also back calculated prefailure shear strengths from the flow failure cases. Similar to the strength ratio analyses, the failure surface search option of *UTEXAS3* and Spencer's (1967) stability method were used to back calculate the mobilized shear strengths from prefailure geometries. A single value of shear strength was assigned to the liquefiable soil, and this value was

Table 1. Case Histories of Liquefaction Flow Failure and Triggering Mechanisms

Case history	Structure	Apparent cause of sliding[a]	Triggering mechanism	Approximate a_{max} (g)
1	Zeeland—Vlietepolder	1889 High tide	Static	
2	Wachusett Dam—north dike	1907 Reservoir filling	Static	
3	Calaveras Dam	1918 Construction	Static	
4	Sheffield Dam	1925 Santa Barbara Eq. (M_L=6.3)	Seismic	0.15
5	Helsinki Harbor	1936 Construction	Static	
6	Fort Peck Dam	1938 Construction	Deformation	
7	Solfatara Canal Dike	1940 Imperial Valley Eq. (M_L=7.1)	Seismic	>0.3
8	Lake Merced bank	1957 San Francisco Eq. (M_L=5.3)	Seismic	>0.12
9	Kawagishi-Cho building	1964 Niigata Eq. (M_W=7.5)	Seismic	0.16
10	Uetsu Railway embankment	1964 Niigata Eq. (M_W=7.5)	Seismic	~0.2
11	El Cobre Tailings Dam	1965 Chilean Eq. (M_L=7 to 7.25)	Seismic	~0.8
12	Koda Numa Highway embankment	1968 Tokachi-Oki Eq. (M_L=7.9)	Seismic	n/a[b]
13	Metoki Road embankment	1968 Tokachi-Oki Eq. (M_L=7.9)	Seismic	n/a[b]
14	Hokkaido Tailings Dam	1968 Tokachi-Oki Eq. (M_L=7.9)	Seismic	n/a[b]
15	Lower San Femando Dam	1971 San Femando Eq. (M_W=6.6)	Seismic	0.5–0.6
16	Tar Island Dyke	1974 Construction	Static	
17	Mochi-Koshi Tailings Dam—Dike 1	1978 Izu-Oshima-Kinkai Eq.	Seismic	0.25–0.35
18	—Dike 2	(M_L=7.0)	Seismic	0.25–0.35
19	Nerlerk Berm—Slide 1	1983 Construction	Deformation	
20	—Slide 2		Deformation	
21	—Slide 3		Deformation	
22	Hachiro-Gata road embankment	1983 Nihon-Kai-Chubu Eq. (M=7.7)	Seismic	0.17
23	Asele road embankment	1983 Pavement repairs	Dynamic[c]	
24	La Marquesa Dam—U/S slope	1985 Chilean Eq. (M_s=7.8)	Seismic	0.6
25	—D/S slope		Seismic	0.6
26	La Palma Dam	1985 Chilean Eq. (M_s=7.8)	Seismic	0.46
27	Fraser River Delta	1985 Gas desaturation and low tide	Static	
28	Lake Ackerman highway embankment	1987 Seismic reflection survey	Dynamic	
29	Chonan Middle School	1987 Chiba-Toho-Oki Eq. (M=6.7)	Seismic	0.12
30	Nalband railway embankment	1988 Armenian Eq. (M_s=6.8)	Seismic	0.5–1.0
31	Soviet Tajik—May 1 slide	1989 Tajik, Soviet Union Eq. (M_L=5.5)	Seismic	0.15
32	Shibecha-Cho embankment	1993 Kushiro-Oki Eq. (M=7.8)	Seismic	0.38
33	Route 272 at Higashiarekinai	1993 Kushiro-Oki Eq. (M=7.8)	Seismic	>0.3

[a]M_L=local (Richter) magnitude, M_W=moment magnitude, M_s=surface wave magnitude, M=magnitude scale not reported.

[b]n/a=not available.

[c]Dynamically induced flow failures are grouped with deformation-induced flow failures for analysis because of higher frequency of motion experienced with respect to seismically induced flow failures.

varied until a factor of safety of unity was achieved. Appropriate fully mobilized drained or undrained shear strengths were assigned to the nonliquefied soils, i.e., progressive failure was not considered. This method is identical to that used by Castro et al. (1989) and Seed et al. (1989) to estimate the prefailure static shear stress in the liquefiable upstream hydraulic fill prior to the 1971 failure of Lower San Fernando Dam. Olson et al. (2000) used this method to estimate the yield shear strength of the liquefied soil from the North Dike of Wachusett Dam. Olson (2001) presents the details of these analyses for each case history.

Flow Failure Case History Back Analysis Results

In 30 of the 33 flow failure cases studied, sufficient information regarding the prefailure conditions was available to conduct stability analyses. [All 33 cases are presented in the following tables so that the numbering of case histories is consistent with Olson (2001) and Olson and Stark (2002).] Table 1 presents the liquefaction flow failures, the triggering mechanism, and available seismic parameters for the seismically induced failures. Olson (2001) and Olson and Stark (2002) provide references for the case histories; therefore, the references are not repeated herein. Table 2 presents the prefailure shear strengths and strength ratios, and weighted average prefailure vertical effective and total stresses for the critical failure surface. Upper and lower bounds of shear strength and strength ratio also are presented in Table 2.

The values of prefailure σ'_{v0}(ave) reported herein for prefailure strength ratio analyses differ from the values of prefailure σ'_{v0}(ave) reported for liquefied strength ratio analyses [i.e., compare Table 2 herein with Table 2 of Olson and Stark (2002)]. Olson (2001) and Olson et al. (2000) indicate that following the initial triggering of liquefaction, it is likely that more soil liquefies and participates in the flow failure, resulting in differences in σ'_{v0}(ave) from the two analyses. This is particularly true in cases of retrogressive failure, such as Vlietepolder (case 1), Helsinki Harbor (case 5), and the Nerlerk failures (cases 19–21).

Table 3 presents the measured and estimated values of CPT and SPT penetration resistance as well as selected soil properties

Table 2. Back Calculated Shear Strengths and Strength Ratios from Flow Failure Case Histories

Case History	Prefailure geometry strength ratio			Prefailure geometry shear strength			Weighted average prefailure vertical effective stress (kPa)	Weighted average prefailure vertical total stress[a] (kPa)
	Best estimate	Lower bound	Upper bound	Best estimate (kPa)	Lower bound (kPa)	Upper bound (kPa)		
1	0.265	0.247	0.28	16.1	15.0	16.8	59.7	—
2	0.26	0.26	0.30	37.6	37.6	41.9	141.6	—
3	0.27	0.255	0.295	76.6	71.8	80.7	294.3	—
4	0.228	0.207	0.249	15.4	12.7	18.0	68.4	84.3
5	0.24	0.21	0.26	3.8	2.2	4.4	15.1	—
6	0.255	0.23	0.285	82.9	69.9	89.6	319.7	—
7	0.225	0.172	0.25	6.0	3.9	6.75	26.5	37.8
8	0.32	0.30	0.34	17.7	15.7	18.1	55.4	89.1
9	—	—	—	—	—	—	—	—
10	0.21	0.19	0.24	10.9	10.0	11.9	51.7	59.4
11	—	—	—	—	—	—	—	—
12	0.24	0.225	0.27	5.3	4.5	5.7	20.9	23.9
13	0.25	0.2	0.29	9.0	8.5	11.1	34.8	42.9
14	0.195	0.155	0.21	11.7	10.3	12.7	59.9	70.2
15	—	—	—	—	—	—	—	—
16	0.265	0.195	0.30	35.9	32.3	38.6	135.8	—
17	0.27	0.24	0.30	21.1	18.0	23.9	73.8	116.1
18	0.22	0.16	0.25	16.0	10.5	18.7	69.2	110.0
19	0.21	0.17	0.23	2.7	2.7	4.0	12.7	—
20	0.21	0.19	0.23	4.2	4.0	4.8	19.8	—
21	0.20	0.165	0.23	4.8	4.2	5.7	24.7	—
22	0.16	0.115	0.205	4.8	4.3	5.3	30.2	36.9
23	0.28	0.22	0.37	16.8	13.9	18.9	59.9	—
24	0.20	0.155	0.27	9.3	6.7	13.4	46.0	101.0
25	0.25	0.195	0.30	12.9	7.7	15.6	51.4	58.4
26	0.26	0.245	0.32	10.1	9.1	12.2	39.7	57.6
27	—	—	—	—	—	—	—	—
28	0.245	0.22	0.275	10.1	8.6	10.5	40.4	—
29	0.215	0.20	0.235	12.2	12.0	12.9	56.4	64.8
30	0.18	0.155	0.21	8.9	8.6	9.6	48.9	78.8
31	0.30	0.28	0.32	31.6	30.4	32.3	106.0	170.4
32	0.24	0.21	0.32	15.8	14.8	18.7	66.6	81.7
33	0.25	0.25	0.255	13.1	13.0	13.4	52.3	71.1

[a]Determined for seismic loading-induced flow failures only.

for each case history. For cases where either CPT or SPT penetration alone was measured, the corresponding value of the other penetration resistance was estimated using the q_c/N_{60} relationship proposed by Stark and Olson (1995) and the median grain size of the liquefied soil. Olson (2001) describes the back analyses conducted, the evaluation of penetration resistance, and the uncertainties and assumptions for each case history.

Flow Failures Triggered by Static Loading

As discussed previously, the shear strength and strength ratio mobilized at the triggering of liquefaction are equal to the yield shear strength and yield strength ratio, respectively, for flow failures triggered by static loading. The authors examined five cases of static loading-induced liquefaction flow failure (cases 1–3, 5, and 16) with sufficient documentation to conduct the proposed back analysis. Fig. 3 presents the values of s_u(yield) and σ'_{v0}(ave) (with upper and lower bounds of each parameter) for these flow failures. Yield strength ratios ranged from approximately 0.24 to 0.30, likely due to differences in relative density, the ratio of horizontal to vertical effective stress, and other factors. The increase in yield strength ratio is subsequently described by increasing penetration resistance.

Flow Failures Triggered by Deformation/Global Instability

Six cases of deformation-induced (or dynamic loading-induced) flow failure (cases 6, 19–21, 23, and 28) are presented in Tables 1 through 3. The authors suspect that the prefailure conditions at Fort Peck Dam (case 6) correspond to the yield strength envelope because deformation occurred simultaneously with fill placement. Also, the dynamic loading-induced flow failures (cases 23 and 28) are grouped with the deformation induced flow failures because of the higher frequency of motion and lower levels of induced shear strain experienced with respect to seismically induced flow failures. As such, prefailure conditions for these two cases likely correspond to the yield strength envelope.

Prefailure conditions for the Nerlerk berm failures (cases 19–21) likely do not correspond to the yield strength envelope be-

Table 3. Measured and Estimated Penetration Resistances for Liquefaction Flow Failure Case Histories

		Normalized penetration resistance						Soil grain properties			
Case history	Available data[a]	Mean q_{c1} (MPa)	Lower bound q_{c1} (MPa)	Upper bound q_{c1} (MPa)	Mean $(N_1)_{60}$ (blows/0.3 m)	Lower bound $(N_1)_{60}$ (blows/0.3 m)	Upper bound $(N_1)_{60}$ (blows/0.3 m)	Reported D_R (%)	Approximate D_{50} (mm)	Approximate FC[b] (%)	Stark and Olson (1995) q_c/N_{60}
1	CPT	3.0	1.7	4.4	7.5	4.2	10.9	—	0.12	3–11	0.4
2	SPT	4.6	2.6	6.5	7	4	10	—	0.42	5–10	0.65
3	D_R	5.5	1	6	8	2	12	20–50	—	10–>60	~0.5
4	D_R	2.2	1.8	2.6	5	4	6	20–40	0.10	33–48	0.35
5	Est.	4.0	—	—	6	—	—	~40	—	—	~0.5
6	SPT	3.4	1.6	5.6	8.5	4	14	40–50	0.06–0.2	~55	0.3–0.5
7	D_R	2.5	—	—	4	—	—	~32	0.17	6–8	0.47
8	D_R;SPT	3.2	3	6.2	7.5	6.5	12.3	~40	0.21 (0.18–0.25)	1–4	0.5 (0.48–0.55)
9	CPT;SPT	3.1	1.7	3.8	4.4	3.7	5.6	~40–50	0.35	<5	0.59
10	Est.	1.8	—	—	3	—	—	—	0.3–0.4	0–2	0.6 (0.57–0.62)
11	SPT	0	—	—	0	—	—	—	0.08–?? (desiccated to NC tailings)	55–93	0.3–??
12	Est.	1.35	—	—	3	—	—	—	0.15–0.20	~13	~0.45
13	Est.[c]	1.05	0.9	1.2	2.6	2.3	3	—	silty sand		~0.4
14	CPT	0.36	0.35	0.38	1.1	1	1.2	—	~0.074	~50	~0.32
15	CPT;SPT	4.7	2.1	6.2	11.5	5	15	~48 (d/s)	sandy silt-silty sand ~0.074 (0.02–0.3)	~50 (5–90)	~0.32
16	CPT;SPT	3.0	2	4	7	4	15	~30–40	~0.15	~10–15	~0.45
17	CPT;SPT	0.5	0.25	1	2.7	0	6	—	0.04	85	0.28
18	CPT;SPT	0.5	0.25	1	2.7	0	6	—	0.04	85	0.28
19	CPT	4.5	2.6	7.8	8.7	5	15	~30–50	0.22	2–12	0.52
20	CPT	3.8	1.9	8.0	7.2	3.6	15.3	~30–50	0.22	2–12	0.52
21	CPT	3.8	1.9	8.0	7.2	3.6	15.3	~30–50	0.22	2–12	0.52
22	CPT;SPT	3.0	1.1	4.9	4.4	3.1	5.8	—	0.2	10–20	0.5
23	SPT	4.0	3.4	4.6	7	6	8	—	0.3 (0.15–0.55)	32 (23–38)	0.57
24	SPT	2.0	1.8	2.3	4.5	4	5	—	~0.15	~30	~0.45
25	SPT	4.1	3.2	5	9	7	11	—	~0.15	~20	~0.45
26	SPT	1.8	1.0	2.5	3.5	2	5	—	~0.2	~15	~0.5
27	CPT	2.9	1.3	4.5	5.3	2.4	8.2	−25 to +5	0.25	0–5	0.55
28	SPT	1.9	0.6	4.4	3	1	7	~0	0.4	0	0.63
29	SPT	2.6	1.8	4.4	5.2	2.6	9	—	~0.2	18	~0.5
30	SPT	6.0	2.3	8.1	9.2[d]	3.6[d]	12.4[d]	—	~1.5	~20	0.65[e]
31	CPT	1.9	1.1	2.4	7.6	4.4	9.6	—	0.012	100	0.25
32	Est.[c]	2.8	1.5	5.4	5.6	2.9	10.7	—	0.2 (0.12–0.4)	20 (12–35)	0.5
33	SPT	3.2	1.2	5.0	6.3	2.4	10	—	~0.2[f]	20[f]	~0.5

[a]CPT=measured cone penetration resistance; SPT=measured standard penetration resistance; D_R=relative density; Est.=estimated.

[b]FC=fines content.

[c]Values of SPT and CPT penetration resistance were estimated from measured Swedish cone penetration test results.

[d]Values of N_{60} were corrected for gravel content as described in Terzaghi et al. (1996).

[e]q_c/N_{60} determined from data presented (Yegian et al. 1994); D_{50} is outside range reported by Stark and Olson (1995).

[f]Values of D_{50} and FC were estimated from same parent soil deposit described by Miura et al. (1998).

cause failure and large strains were initiated in an underlying foundation layer of soft clay (Been et al. 1987; Rogers et al. 1990) while filling was stopped. However, Sladen et al. (1987) suggested that this mechanism does not explain the postfailure morphology of the berm. The authors suspect that global failure initiated in the foundation clay, and this caused sufficient deformation in the berm sands to trigger liquefaction. The analysis by Hicks and Boughrarou (1998) supports this failure mechanism. Therefore, the prefailure strength ratios back calculated for cases 19–21 likely are considerably lower than the yield strength ratios.

Fig. 3 includes the values of prefailure shear strength and σ'_{v0}(ave) (with upper and lower bounds of each parameter) for these six cases. Prefailure strength ratios for these six cases ranged from approximately 0.20 to 0.28.

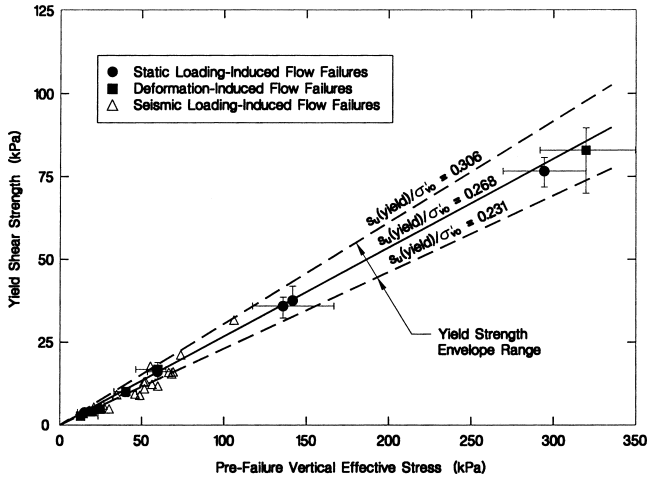

Fig. 3. Comparison of yield and mobilized shear strength and prefailure vertical effective stress for static loading-induced, deformation-induced, and seismically induced flow failures (for clarity, ranges only shown for static loading- and deformation-induced failures)

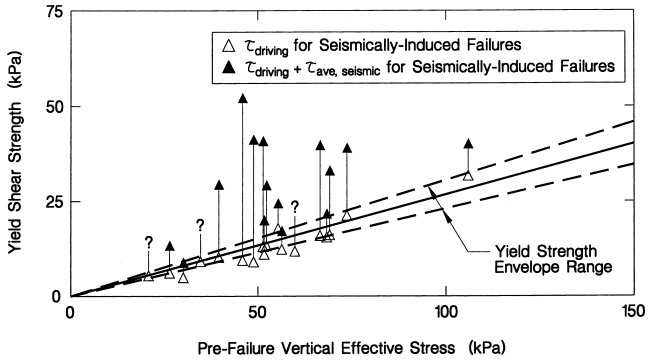

Fig. 4. Comparison of static driving shear stress and combined static and seismic shear stresses for seismically induced flow failures with yield strength envelope

Flow Failures Triggered by Seismic Loading

The shear strength and strength ratio back calculated from flow failures triggered by seismic loading generally are less than the corresponding yield shear strength and strength ratio, respectively. However, if the shear stress ratio existing prior to flow failure is near the yield strength ratio, only a small seismic disturbance is required to trigger liquefaction. On the other hand, if the static shear stress ratio is considerably smaller than the yield strength ratio, considerable deformation and porewater pressure increase during shaking are required to trigger liquefaction. Nineteen cases of seismically induced liquefaction flow failure are presented in Tables 1 through 3. Prefailure strength ratios for these 19 cases ranged from approximately 0.15 to 0.32. These data are included in Fig. 3 *for comparison only* and were not used to develop the proposed yield strength envelope.

To evaluate the effect of seismic loading on these 19 case histories, the cyclic stress method proposed by Seed and Idriss (1971) for level ground was used to estimate the average seismic stresses and stress ratios. As the large majority of the cases studied involved slopes and embankments smaller than 10 m in height, the authors anticipate that the effect of sloping ground on the seismic stresses is minimal. For cases of larger slopes and embankments, the liquefiable soil was located at depths considerably below the surface of the slope or embankment. Based on Makdisi and Seed (1978), the authors anticipate that there is minimal amplification of the free-field shear stresses in the zone of liquefaction at depth within the slope or embankment. In addition, the cyclic stress equation provides the only means to evaluate the seismically induced failures because insufficient information is available regarding the seismic loads and dynamic properties of the materials to conduct more detailed analyses.

Average sustained seismic shear stress and stress ratio were calculated as follows:

$$\tau_{\text{ave,seismic}} = \left(0.65 \cdot \frac{\alpha_{\max}}{g} \cdot \sigma_{v0}(\text{ave}) \cdot r_d\right) \Big/ C_M \qquad (3a)$$

$$\frac{\tau_{\text{ave,seismic}}}{\sigma'_{v0}(\text{ave})} = \left(0.65 \cdot \frac{\alpha_{\max}}{g} \cdot \frac{\sigma_{v0}(\text{ave})}{\sigma'_{v0}(\text{ave})} \cdot r_d\right) \Big/ C_M \qquad (3b)$$

where $\alpha_{\max}$=peak free-field surface acceleration (see Table 1); g=acceleration of gravity; and r_d=depth reduction factor [calculated using the equation proposed by Youd and Idriss (1997) and the average depth of the critical failure surface within the zone of liquefaction]; and C_M=lower bound of the range of magnitude scaling factors recommended by Youd and Idriss (1997).

The open triangles in Fig. 4 represent the prefailure static shear and vertical effective stresses prior to seismic loading in the seismically induced failures. The solid triangles in Fig. 4 represent the combined static and sustained seismic shear stresses (at the same prefailure vertical effective stress). The yield strength envelope (developed using the static loading-induced failures) from Fig. 3 also is included in Fig. 4. It can be seen that the combined static and sustained seismic shear stresses for the seismic cases exceed the mean yield strength envelope. This suggests that liquefaction would be triggered in each seismic case history.

It is understood that the effect of seismic loading would be represented more accurately by the induced porewater pressure increase or induced shear strain instead of the cyclic stress equation. However, using the sustained seismic shear stress ($0.65\tau_{\max,\text{seismic}}$) normalized to 15 cycles of uniform shaking (using C_M) rather than the maximum seismic shear stress (which may occur only once during shaking) suggests that this seismic shear stress is sustained for a sufficient number of cycles to cause substantial porewater pressure increase. Further, the simplicity of this procedure and the correct prediction of liquefaction for all the seismically induced flow failures (see Fig. 4) justify the approach. The authors currently are developing improved methods to evaluate porewater pressure increase resulting from seismic loading for use in back analysis and design.

Yield Strength Ratio and Penetration Resistance

Fig. 5 presents the best estimates of yield strength ratio and mean q_{c1} value (from Tables 2 and 3) for the flow failures. Similarly, Fig. 6 presents the best estimates of yield strength ratio and mean $(N_1)_{60}$ value. The seismic cases are included in these figures *for comparison only*. These data were not used to develop the proposed relationships. For each case history, the range of back-calculated strength ratio and measured (or estimated) penetration resistance is presented in Tables 2 and 3. The ranges result from uncertainties regarding: (1) the shear strength of nonliquefied soils; (2) the location of the initial failure surface; (3) the dimensions of the zone of liquefaction; and (4) the location of the

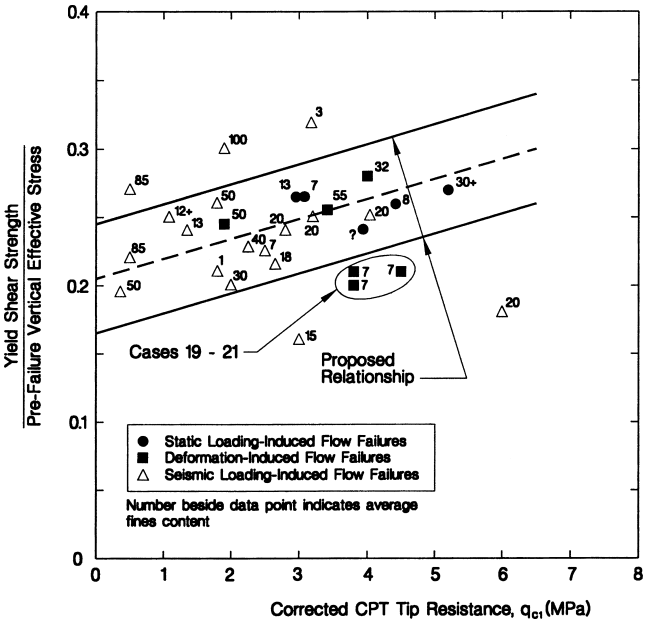

Fig. 5. Comparison of yield and mobilized strength ratios and corrected CPT tip resistance for liquefaction flow failures

phreatic surface, among other factors. Olson (2001) describes the uncertainties and assumptions made for each case history.

Despite the uncertainties, a trend of increasing yield strength ratio with increasing penetration resistance is observed in Figs. 5 and 6 for the static loading- and deformation-induced failures (plotted as solid circles and squares, respectively), excluding the Nerlerk berm cases (cases 19–21). It can be seen that a few of the seismically induced flow failures plot above the average trend of the static loading-induced failures. Therefore, there may be greater variability in the relationship between yield strength ratio and penetration resistance than that indicated by the static loading-induced cases. As a result, the upper and lower trendlines

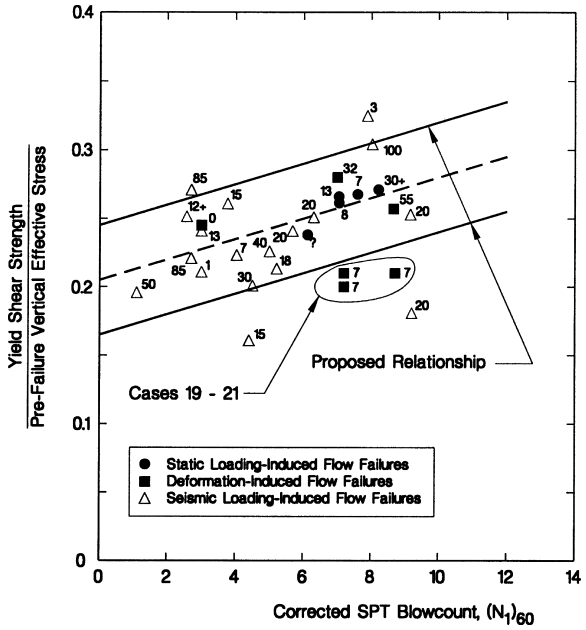

Fig. 6. Comparison of yield and mobilized strength ratios and corrected SPT blowcount for liquefaction flow failures

were positioned conservatively to account for this variability. The proposed average trendlines are described as

$$\frac{s_u(\text{yield})}{\sigma'_{v0}} = 0.205 + 0.0143(q_{c1}) \pm 0.04 \quad \text{for } q_{c1} \lesssim 6.5 \text{ MPa} \tag{4a}$$

$$\frac{s_u(\text{yield})}{\sigma'_{v0}} = 0.205 + 0.0075[(N_1)_{60}] \pm 0.04 \quad \text{for } (N_1)_{60} \lesssim 12 \tag{4b}$$

Effect of Fines Content on Yield Shear Strength

Referring to Table 3, it is clear that many of the case histories involved silty sands. The fines contents of the individual cases are plotted beside the yield strength ratio in Figs. 5 and 6. As expected, the data reveal no trend in yield strength ratio with respect to fines content. Data presented by numerous investigators (e.g., Kuerbis et al. 1988; Pitman et al. 1994; Ovando-Shelley and Perez 1997; Yamamuro et al. 1999; Olson 2001) for a large number of sandy soils indicate that the presence of fines has little effect on the yield shear strength (which is mobilized at small strains). This differs from behavior often observed at large strain, where fines content can affect the liquefied shear strength.

Increasing fines content is generally considered to decrease penetration resistance of sandy soils as a result of increasing soil compressibility and decreasing permeability. However, the fines involved in the failures studied herein are typically nonplastic or low plasticity, and may have only a moderate influence on penetration resistance. As a result, no fines content adjustment is recommended for evaluating the yield shear strength. However, the cone penetration tip resistance, q_c, should be corrected for unequal end area effects (i.e., corrected to q_T) for use in the proposed relationships.

Liquefaction Analysis Procedure

Using values of yield and liquefied strength ratio back-calculated from liquefaction flow failures, Olson (2001) proposed a comprehensive liquefaction analysis for ground subjected to a static shear stress. This procedure addresses liquefaction susceptibility, triggering of liquefaction, and post-triggering/flow failure stability. Olson and Stark (2001) utilized this procedure to successfully predict the historic behavior of Lower San Fernando Dam.

Liquefaction Flow Failure Susceptibility

The first step of a liquefaction analysis for sloping ground is to determine if the soil is contractive, i.e., susceptible to flow failure. Fig. 7 presents SPT based flow failure susceptibility relationships from the literature with the case history data. The prefailure σ'_{v0} plotted in Fig. 7 (and also in Fig. 8) is the average of the values of σ'_{v0}(ave) from the yield strength ratio analysis (see Table 2) and the liquefied strength ratio analysis [see Table 2 of Olson and Stark (2002)]. Fear and Robertson (1995) presented a susceptibility boundary relationship using critical state soil mechanics theory and laboratory test results, and their boundary encompasses all but one of the mean $(N_1)_{60}$ values for the case histories. Based on the agreement with theory, laboratory results, and field case histories, the Fear and Robertson (1995) boundary is recommended for practice to delineate field conditions susceptible and not susceptible to flow failure. Similarly, Fig. 8 presents CPT

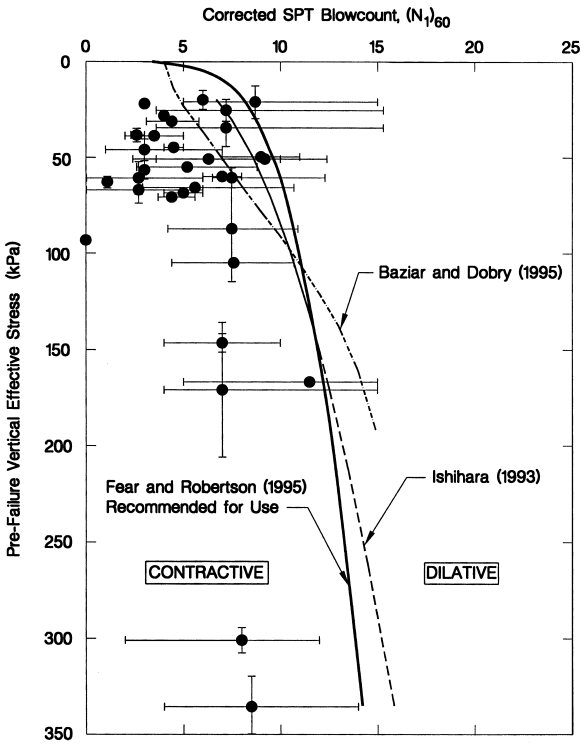

Fig. 7. Relationships separating contractive from dilative conditions using flow failure case histories and corrected SPT blowcount (bars indicate ranges of penetration test values and prefailure effective stresses)

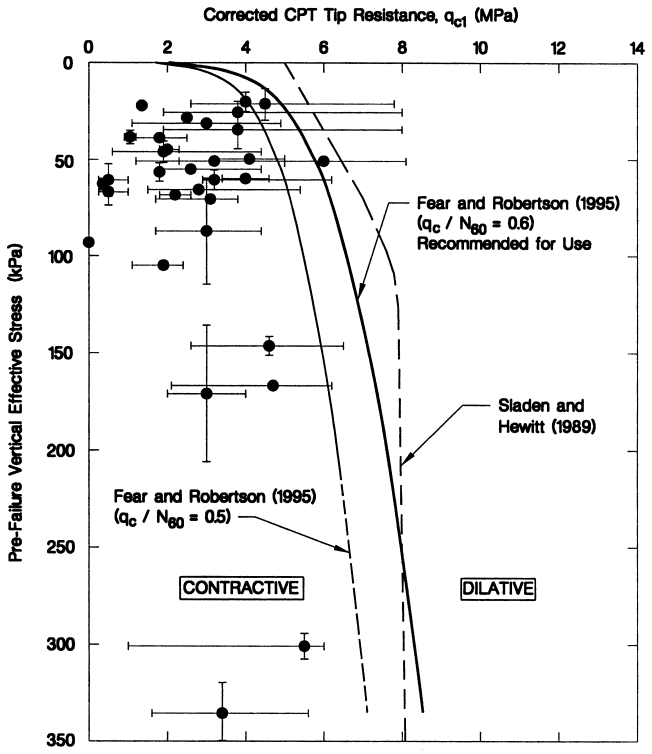

Fig. 8. Relationships separating contractive from dilative conditions using flow failure case histories and corrected CPT tip resistance (bars indicate ranges of penetration test values and prefailure vertical effective stresses)

based liquefaction susceptibility relationships from the literature with the case history data. The Fear and Robertson (1995) boundary (converted to CPT) encompasses all but one of the mean q_{c1} data for the case histories and is therefore recommended for practice. The Fear and Robertson (1995) boundary was converted to CPT using $q_c/N_{60}=0.6$, obtained from Stark and Olson (1995) for a median D_{50} typical for clean sands. The recommended boundary relations can be approximated as:

$$(\sigma'_{v0})_{\text{boundary}}=9.58\times 10^{-4}[(N_1)_{60}]^{4.79} \quad (5a)$$

$$(\sigma'_{v0})_{\text{boundary}}=1.10\times 10^{-2}(q_{c1})^{4.79} \quad (5b)$$

where σ'_{v0} and q_{c1} have units of kPa and MPa, respectively.

In the design of new structures or evaluation of existing structures, records of q_{c1} and/or $(N_1)_{60}$ should be plotted against vertical effective stress. These plots should include the corresponding recommended liquefaction susceptibility relationship [Eq. (5*a*) or Eq. (5*b*)]. The susceptibility relations can be incorporated into a spreadsheet file that contains the penetration data. Using these plots, layer(s) of soil that are contractive (and therefore susceptible to flow failure) can be identified. With sufficient field penetration tests, zones of contractive soil can be delineated in two and three dimensions.

Triggering Analysis

The next step is to determine whether the combined static, seismic, and/or other shear stresses exceed the yield shear strength of the contractive soil(s). This is accomplished using the following procedure, which can be incorporated into a spreadsheet program. Olson (2001) and Olson and Stark (2001) illustrate the ease and functionality of this step.

1. Conduct a slope stability backanalysis of the prefailure geometry to estimate the static shear stress (τ_{driving}) in the contractive (liquefiable) soil(s). A trial value of shear strength is assumed for the liquefiable soils, and the shear strength assigned to the liquefiable soils is modified until a factor of safety of unity is achieved. Fully mobilized drained or undrained shear strengths are assigned to the nonliquefiable soils. The slope stability search should consider both circular and noncircular potential failure surfaces.
2. Divide the critical failure surface into a number of segments. Based on analyses conducted for this study, ten to fifteen segments are satisfactory.
3. Determine the weighted average value of σ'_{v0} along the critical failure surface and calculate the average static shear stress ratio, $\tau_{\text{driving}}/\sigma'_{v0}(\text{ave})$. Alternately, $\tau_{\text{driving}}/\sigma'_{v0}(\text{ave})$ may be estimated from some commercially available slope stability software that allows layer shear strengths to be input as strength ratios, i.e., s_u/σ'_{v0}. Use of such an option can simplify this procedure.
4. Estimate the average seismic shear stress ($\tau_{\text{ave,seismic}}$) applied to each segment of the critical failure surface using Eq. (3*a*) or a site response analysis.
5. If applicable, estimate other shear stresses (τ_{other}) applied to each segment of the critical failure surface using appropriate analyses.
6. Determine the value of $s_u(\text{yield})/\sigma'_{v0}$ using corrected mean CPT and/or SPT penetration resistance and Eqs. (4*a*) and (4*b*), respectively. The desired level of conservatism can be incorporated by using a penetration resistance larger or

smaller than the mean value, or by selecting a yield strength ratio higher or lower than the mean value.

7. Calculate the values of s_u(yield) and $\tau_{driving}$ *for each segment* of the critical failure surface by multiplying the values of s_u(yield)/σ'_{v0} and $\tau_{driving}/\sigma'_{v0}$(ave) by the σ'_{v0} for the segment, respectively.
8. The factor of safety against the triggering of liquefaction in each segment is then estimated as

$$FS_{Triggering} \approx \frac{s_u(\text{yield})}{\tau_{driving} + \tau_{ave,seismic} + \tau_{other}} \quad (6)$$

Segments with a $FS_{Triggering}$ greater than unity are unlikely to liquefy. If all segments have $FS_{Triggering} > 1$, a post-triggering stability analysis is unnecessary. Segments with $FS_{Triggering} \leq 1$ are likely to liquefy and these segments should be assigned the liquefied shear strength for a post-triggering stability analysis. Segments with $FS_{Triggering} > 1$ should be assigned their yield shear strength for a post-triggering stability analysis. The authors recommend that both the critical circular and noncircular failure surfaces (determined in Step 1 above) be analyzed, as the ratio of $\tau_{driving}/\tau_{ave,seismic}$ may vary between potential failure surfaces. Analyzing both circular and noncircular critical failure surfaces should result in failure surfaces that vary considerably in depth and location within the zone(s) of contractive soil. If the circular and noncircular failure surfaces cross the zone(s) of contractive soil at about the same location and depth, it is recommend that one or two additional potential failure surfaces that cross the zone(s) of contractive soil at different locations be analyzed.

Post-triggering/Flow Failure Stability Analysis

If liquefaction is triggered, a post-triggering stability analysis of the structure (using the prefailure geometry) must be conducted to determine whether the static shear forces are greater than the available shear resistance (including the liquefied shear strength). The liquefied shear strength ratio is estimated from the following relationships proposed by Olson and Stark (2002):

$$\frac{s_u(\text{LIQ})}{\sigma'_{v0}} = 0.03 + 0.0143(q_{c1}) \pm 0.03 \quad \text{for } q_{c1} \leq 6.5 \text{ MPa} \quad (7a)$$

$$\frac{s_u(\text{LIQ})}{\sigma'_{v0}} = 0.03 + 0.0075[(N_1)_{60}] \pm 0.03 \quad \text{for } (N_1)_{60} \leq 12 \quad (7b)$$

Appropriate values of liquefied shear strength are estimated (using the value of σ'_{v0} for the segment) and assigned to the segments of the critical failure surface predicted to liquefy from the triggering analysis. Fully mobilized drained or undrained shear strengths are assigned to the nonliquefied soils. This analysis should be conducted for all of the potential failure surfaces that were examined in the triggering analysis.

If the factor of safety against flow failure, FS_{Flow}, is less than or equal to unity, flow failure of the structure is predicted to occur. However, if the FS_{Flow} is between unity and about 1.1, some deformation is likely, and segments of the failure surface with marginal $FS_{Triggering}$ (less than about 1.1) should be reassigned their liquefied shear strength. The post-triggering stability analysis should be repeated with the new segment shear strengths to determine a new FS_{Flow}. This accounts for the potential for deformation-induced liquefaction and progressive failure of the structure. The minimum FS_{Flow} will be calculated when liquefaction is triggered in all zones of contractive soil and assigned their liquefied shear strengths for the flow failure stability analysis. This condition can be analyzed to determine the worst case FS_{Flow} and to aid judgments regarding the need for redesign or remediation.

Conclusions

There are limitations of existing methods (e.g., Poulos et al. 1985a,b; Seed and Harder 1990) to analyze liquefaction triggering for ground subjected to static shear stress, i.e., sloping ground. This paper proposes an alternate procedure to evaluate the triggering of liquefaction in ground subjected to a static shear stress using the yield strength ratio back calculated from static liquefaction flow failures. The results of the back analyses indicate that there is a nearly linear relationship between yield shear strength (the peak shear strength available at the triggering of liquefaction) and prefailure vertical effective stress for a wide range of effective stress. Back-calculated yield strength ratios ranged from approximately 0.23 to 0.31 and the increase in yield strength ratio is correlated to corrected CPT and SPT penetration resistance.

The proposed liquefaction triggering analysis is incorporated into a comprehensive liquefaction analysis for ground subjected to a static shear stress. The liquefaction analysis is based on yield and liquefied strength ratios backanalyzed from liquefaction flow failures, and consists of the following general steps: (1) evaluate liquefaction susceptibility using proposed relationships between penetration resistance and vertical effective stress that separate contractive from dilative conditions; (2) determine the yield strength ratio using penetration resistance and the relationships proposed herein, and evaluate the triggering of liquefaction by comparing yield shear strength to combined static and additional shear stresses; and (3) if liquefaction is triggered, evaluate the post-triggering stability using a conventional limit-equilibrium analysis of the prefailure geometry and the recommended liquefied shear strengths.

Acknowledgments

This study was funded by the National Science Foundation (NSF), Grant No. 97-01785, as part of the Mid-America Earthquake (MAE) Center headquartered at the University of Illinois at Urbana-Champaign. This support is gratefully acknowledged.

References

Baziar, M. H., and Dobry, R. (1995). "Residual strength and large-deformation potential of loose silty sands." *J. Geotech. Eng.,* 121(12), 896–906.

Been, K., Conlin, B. H., Crooks, J. H. A., Fitzpatrick, S. W., Jefferies, M. G., Rogers, B. T., and Shinde, S. (1987). "Back analysis of the Nerlerk berm liquefaction slides: Discussion." *Can. Geotech. J.,* 24, 170–179.

Castro, G., Keller, T. O., and Boynton, S. S. (1989). "Re-evaluation of the Lower San Fernando Dam: Report 1, an investigation of the February 9, 1971 slide." *U.S. Army Corps of Engineers Contract Rep. No. GL-89-2*, Vols. 1 and 2, U.S. Army Corps of Engineers Waterways Experiment Station, Vicksburg, Miss.

Eckersley, D. (1990). "Instrumented laboratory flow slides." *Geotechnique,* 40, 489–502.

Fear, C. E., and Robertson, P. K. (1995). "Estimating the undrained strength of sand: A theoretical framework." *Can. Geotech. J.,* 32(4), 859–870.

Hanzawa, H. (1980). ''Undrained strength and stability analysis for a quick sand.'' *Soils Found.,* 20(2), 17–29.

Hanzawa, H., Itoh, Y., and Suzuki, K. (1979). ''Shear characteristics of a quick sand in the Arabian Gulf.'' *Soils Found.,* 19(4), 1–15.

Harder, L. F., Jr., and Boulanger, R. (1997). ''Application of K_σ and K_α correction factors.'' *Proc., NCEER Workshop on Evaluation of Liquefaction Resistance of Soils*, T. L. Youd and I. M. Idriss, eds., NCEER-97-0022, 167–190.

Hedien, J. E., Anderson, R. J., and Niznik, J. A. (1998). ''Evaluation of liquefaction potential and seismic safety for Tennessee Valley Authority embankment dams.'' *Proc., Conf. on Current Earthquake Engineering Research in the Central United States* (CEERICUS'98), D. F. Laefer and J. P. Arnett, eds., Univ. of Illinois-Urbana-Champaign, April 4, II-1–II-8.

Hicks, M. A., and Boughrarou, R. (1998). ''Finite element analysis of the Nerlerk underwater berm failures.'' *Geotechnique,* 48(2), 169–185.

Ishihara, K. (1984). ''Post-earthquake failure of a tailings dam due to liquefaction of the pond deposit.'' *Proc., Int. Conf. on Case Histories in Geotechnical Engineering*, Rolla, Mo., May 6–11, 3, 1129–1143.

Ishihara, K. (1993). ''Liquefaction and flow failure during earthquakes.'' *Geotechnique,* 43(3), 351–415.

Kuerbis, R., Negussey, D., and Vaid, Y. P. (1988). ''Effect of gradation and fines content on the undrained response of sand.'' *Hydraulic fill structures*, ASCE Geotechnical Engineering Division Specialty Publication No. 21, D. J. A. Van Zyl and S. G. Vick, eds., Fort Collins, Colo., 330–345.

Makdisi, F. I., and Seed, H. B. (1978). ''Simplified procedure for estimating dam and embankment earthquake-induced deformations.'' *J. Geotech. Eng. Div., Am. Soc. Civ. Eng.,* 104(7), 849–867.

Miura, K., Yoshida, N., Nishimura, M., and Wakamatsu, K. (1998). ''Stability analysis of the fill embankment damaged by recent two major earthquakes in Hokkaido, Japan.'' *Proc., 1998 Geotechnical Earthquake Engineering and Soil Dynamics Specialty Conf.*, ASCE Geo-Institute Geotechnical Specialty Publication No. 75, Vol. 2, August 3–6, Seattle, 926–937.

Olson, S. M. (2001). ''Liquefaction analysis of level and sloping ground using field case histories and penetration resistance.'' PhD thesis, Univ. of Illinois-Urbana-Champaign, Urbana, Ill. 549 p. (available at http://pgi-tp.ce.uiuc.edu/olsonwebfiles/olsonweb/index.htm)

Olson, S. M., Stark, T. D., Walton, W. H., and Castro, G. (2000). ''1907 Static liquefaction flow failure of North Dike of Wachusett Dam.'' *J. Geotech. Geoenviron. Eng.,* 126(12), 1184–1193.

Olson, S. M., and Stark, T. D. (2001). ''Liquefaction analysis of Lower San Fernando Dam using strength ratios.'' *Proc., Fourth Int. Conf. on Recent Advances in Geotechnical Earthquake Engineering and Soil Dynamics*, S. Prakash, ed., San Diego. Paper 4.05.

Olson, S. M., and Stark, T. D. (2002). ''Liquefied strength ratio from liquefaction flow failure case histories.'' *Can. Geotech. J.,* 39, 629–647.

Ovando-Shelley, E., and Perez, B. E. (1997). ''Undrained behavior of clayey sands in load controlled triaxial tests.'' *Geotechnique,* 47(1), 97–111.

Pillai, V. S., and Stewart, R. A. (1994). ''Evaluation of liquefaction potential of foundation soils at Duncan Dam.'' *Can. Geotech. J.,* 31, 951–966.

Pitman, T. D., Robertson, P. K., and Sego, D. C. (1994). ''Influence of fines on the collapse of loose sands.'' *Can. Geotech. J.,* 31, 728–739.

Poulos, S. J. (1988). ''Liquefaction and related phenomena.'' *Advanced dam engineering for design, construction, and rehabilitation*, R. B. Jansen, ed., Van Nostrand Reinhold, New York, 292–320.

Poulos, S. J., Castro, G., and France, W. (1985a). ''Liquefaction evaluation procedure.'' *J. Geotech. Eng.,* 111(6), 772–792.

Poulos, S. J., Robinsky, E. I., and Keller, T. O. (1985b). ''Liquefaction resistance of thickened tailings.'' *J. Geotech. Eng.,* 111(12), 1380–1394.

Rogers, B. T., Been, K., Hardy, M. D., Johnson, G. J., and Hachey, J. E. (1990). ''Re-analysis of Nerlerk B-67 berm failures.'' *Proc., 43rd Can. Geot. Conf.—Prediction of Performance in Geotechnique*, Quebec, Canada, 1, 227–237.

Sasitharan, S., Robertson, P. K., Sego, D. C., and Morgenstern, N. R. (1993). ''Collapse behavior of sand.'' *Can. Geotech. J.,* 30, 569–577.

Seed, R. B., and Harder, L. F., Jr. (1990). ''SPT-based analysis of cyclic pore pressure generation and undrained residual strength.'' *Proc., H.B. Seed Memorial Symp.*, Bi-Tech Publishing Ltd., 2, 351–376.

Seed, H. B., and Idriss, I. M. (1971). ''Simplified procedure for evaluating soil liquefaction potential.'' *J. Soil Mech. Found. Div., Am. Soc. Civ. Eng.,* 97(9), 1249–1273.

Seed, H. B., Seed, R. B., Harder, L. F., and Jong, H.-L. (1989). ''Re-evaluation of the Lower San Fernando Dam: Report 2, examination of the post-earthquake slide of February 9, 1971.'' *U.S. Army Corps of Engineers Contract Rep. No. GL-89-2*, U.S. Army Corps of Engineers Waterways Experiment Station, Vicksburg, Miss.

Seed, H. B., Tokimatsu, K., Harder, L. F., and Chung, R. (1985). ''The influence of SPT procedures in soil liquefaction resistance evaluations.'' *J. Geotech. Eng.,* 111(12), 1425–1445.

Sladen, J. A., D'Hollander, R. D., and Krahn, J. (1985). ''The liquefaction of sands, a collapse surface approach.'' *Can. Geotech. J.,* 22, 564–578.

Sladen, J. A., D'Hollander, R. D., Krahn, J., and Mitchell, D. E. (1987). ''Back analysis of the Nerlerk berm liquefaction slides: Reply.'' *Can. Geotech. J.,* 24, 179–185.

Sladen, J. A., and Hewitt, K. J. (1989). ''Influence of placement method on the in situ density of hydraulic sand fills.'' *Can. Geotech. J.,* 26, 453–466.

Spencer, E. (1967). ''A method of analysis of the stability of embankments assuming parallel inter-slice forces.'' *Geotechnique,* 17(1), 11–26.

Stark, T. D., and Olson, S. M. (1995). ''Liquefaction resistance using CPT and field case histories.'' *J. Geotech. Eng.,* 121(12), 856–869.

Terzaghi, K., Peck, R. B., and Mesri, G. (1996). *Soil mechanics in engineering practice*, 3rd Ed., Wiley, New York.

Vaid, Y. P., and Chern, J. C. (1985). ''Cyclic and monotonic undrained response of saturated sands.'' *Proc., Advances in the Art of Testing Soils under Cyclic Conditions*, V. Khosla, ed., ASCE, New York, 120–147.

Wright, S. G. (1992). *UTEXAS3: A computer program for slope stability calculations*, Geotechnical Engineering Software GS86-1, Dept. of Civil Engineering, Univ. of Texas, Austin.

Yamamuro, J. A., Covert, K. M., and Lade, P. V. (1999). ''Static and cyclic liquefaction of silty sands.'' *Proc., Int. Workshop on the Physics and Mechanics of Soil Liquefaction*, P. V. Lade and J. A. Yamamuro, eds., Baltimore, 55–65.

Yegian, M. K., Ghahraman, V. G., and Harutinunyan, R. N. (1994). ''Liquefaction and embankment failure case histories, 1988 Armenian earthquake.'' *J. Geotech. Eng.,* 120(3), 581–596.

Youd, T. L., and Idriss, I. M., Eds. (1997). ''Summary report.'' *Proc., NCEER Workshop on Evaluation of Liquefaction Resistance of Soils*, NCEER-97-0022, 1–40.